THE JOURNAL OF PHYSICAL CHEMISTRY LETTERS
A JOURNAL OF THE AMERICAN CHEMICAL SOCIETY

pubs.acs.org/JPCL

Letter

Different Charge Transport Mechanisms in $Ti_3C_2T_x$ MXene Monoflakes and Multiflakes

Hui Fang,[§] Zhenyao Fang,[§] Anupma Thakur, Babak Anasori,* Andrew M. Rappe,* and Zahra Fakhraai*

Cite This: *J. Phys. Chem. Lett.* 2025, 16, 7515−7521

Read Online

ACCESS | Metrics & More | Article Recommendations | Supporting Information

ABSTRACT: MXenes have demonstrated their potential for various electronic and optoelectronic applications. However, our understanding of MXene charge transport mechanisms remains rather incomplete. Here, we provide a unifying picture of charge transport in monoflake and multiflake MXenes by measuring and calculating their temperature-dependent resistivity. We measure a positive temperature-dependent resistivity for both monoflakes and the out-of-plane direction of stacked multiflakes of $Ti_3C_2T_x$ MXenes, indicating that charge transport is predominantly band-like. In contrast, a negative temperature-dependent resistivity is observed in the in-plane direction of multiflake MXenes, suggesting that charge transport is governed by thermally activated interflake hopping, which is facilitated by the presence of trapped water. These findings provide insight into the precise role of trapped water in $Ti_3C_2T_x$ MXene resistivity, opening avenues for controlling charge transport in electronic and optoelectronic applications, especially in extremely high temperature environments.

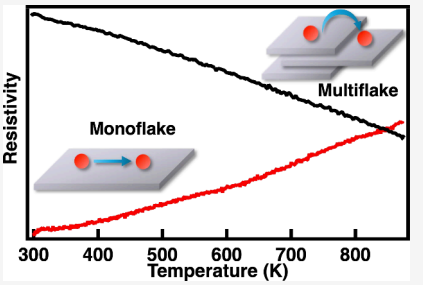

MXenes have demonstrated significant potential for a wide range of electronic and optoelectronic applications[1−4] because they possess outstanding electronic, optical, and mechanical properties.[1,5,6] MXenes have the general chemical formula of $M_{n+1}X_nT_x$ (n = 1−4), where M represents a transition metal, X represents carbon and/or nitrogen, and T_x represents surface terminations (typically −F, −Cl, =O, and −OH).[1] Their diversity in surface termination, ease of functionalization, and stoichiometric composition result in various tunable properties, broadening their potential applications.[7−11]

MXenes have a high free carrier density (10^{21}−10^{22} cm^{-3}),[12] making them excellent candidates for electronic and optoelectronic devices.[1,13] Understanding the carrier transport mechanisms governing the conductivity is critical for these applications.[14,15] Temperature-dependent conductivity measurements have been used to understand the charge transport mechanism, but the results are not consistent across various methods and synthesis conditions.[14,16,17] Both thermally activated hopping (conductivity increasing with increasing temperature)[16,18] and band-like conductivity (conductivity decreasing with increasing temperature)[14,17] have been proposed for metallic $Ti_3C_2T_x$ MXenes. Possible reasons for these differences include differences between various measurement and modeling techniques or the choice of sample geometry.[19,20] In single-flake samples, intraflake conductivity is measured, while in multiflake samples or bulk samples, interflake conductivity is dominant.[21,22] In multiflakes, variations in surface terminations and the amount of intercalated water can play a more significant role in determining conductivity,[16,22] as charge hopping between flakes can play a more prominent role.

Intercalated water plays a significant role in MXene conductivity by acting as a bridge for the charge transport between MXene layers. The interflake resistivity of thick MXene films at room temperature, with a thickness of several micrometers, was found to increase as the water was deintercalated.[16,20,23] These observations indicate that water, which is a dielectric, can act as a barrier for charge transport in the out-of-plane direction. Additionally, the surface terminations and intercalated ions or molecules also significantly influence conductivity.[22,24] Previous work demonstrated that $Ti_3C_2T_x$ MXenes with =O surface termination have lower conductivity than those with −OH surface terminations.[22] The conductivity of $Ti_3C_2T_x$ MXenes was also reported to decrease as the interflake spacing increases, which can be controlled by interactions with different ions or molecules.[24] These observations suggest that conductivity and its temperature dependence could also be altered in both multiflake and monoflake MXene films as their surface termination and the amount of intercalated water are varied.

In this work, we investigate the charge transport mechanisms of $Ti_3C_2T_x$ MXene films through studies of the temperature-

Received: May 12, 2025
Revised: June 23, 2025
Accepted: July 10, 2025
Published: July 18, 2025

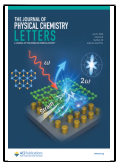

https://doi.org/10.1021/acs.jpclett.5c01439
J. Phys. Chem. Lett. 2025, 16, 7515−7521

dependent resistivity by spectroscopic ellipsometry (SE) measurements and DFT calculations. We demonstrate that intraflake transport processes govern the band-like charge transport in monoflakes. However, in-plane interflake charge hopping transport plays a more dominant role in stacked multiflakes; hopping transport is activated at elevated temperatures and can be assisted by the trapped water, which acts to reduce resistivity. Our results demonstrate the important role of electron−phonon coupling and interflake charge transport in $Ti_3C_2T_x$ MXene conductivity and reconcile the previous debates, broadening the possibility of using MXenes in high-temperature electronic and optoelectronic applications.

$Ti_3C_2T_x$ MXene was synthesized by selective etching of the optimized Ti_3AlC_2 MAX phase[25] using a mixed acid (HF−HCl) approach and delaminated using LiCl. Details can be found in the Materials and Methods section of the SI and our previous work.[26] $Ti_3C_2T_x$ MXene thin films of different thicknesses were spin-coated on a Si substrate coated with 300 nm thermally evaporated SiO_2 from an aqueous solution (details in Materials and Methods and previous work[27]).

To determine the optical properties of the $Ti_3C_2T_x$ MXene films, variable-angle SE measurements were performed at room temperature.[28] An example of the measured spectroscopic angles $\Psi(\lambda)$ and $\Delta(\lambda)$ (λ is the wavelength) for the as-prepared $Ti_3C_2T_x$ MXene film coated on a 300 nm SiO_2/Si substrate with ∼2 nm thickness is shown in Figure 1A,B. The SE results for thicker films are presented in Figure S1. The

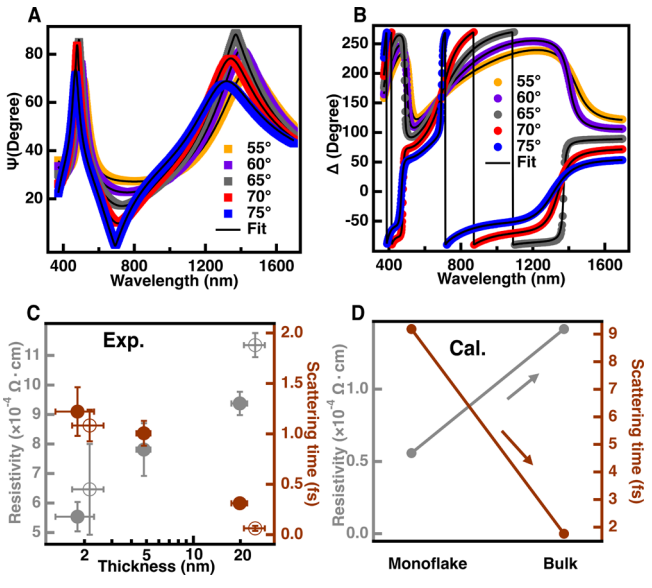

Figure 1. Spectroscopic ellipsometry measurements. (A, B) Measured spectroscopic angles Ψ (A, squares) and Δ (B, spheres) along with the global best fit (solid black lines in both figures) as a function of wavelength at various angles of incidence [55° (orange), 60° (purple), 65° (gray), 70° (red), and 75° (blue)] performed on an optimized-$Ti_3C_2T_x$ monoflake film with a thickness of ∼2 nm coated on a 300 nm SiO_2/Si substrate. (C) Experimentally deduced resistivity (gray, left axis) and scattering time (brown, right axis) of $Ti_3C_2T_x$ MXene films vs film thickness. Filled symbols show multiangle data on 300 nm SiO_2/Si substrates, and open symbols show averaged mapping data collected on Si, respectively. (D) DFT-calculated electrical resistivity (gray, left axis) and electron scattering time (brown, right axis) of the monoflake and the in-plane component (*xx* component) of bulk $Ti_3C_2O_2$ with intercalated water, considering electron−phonon coupling.

fitting details are described in Supplementary Note S1, and the fitting results are tabulated in Table S1. We note that data at all angles are fitted simultaneously with an isotropic optical model. As detailed in Supplementary Note S1, fitting anisotropy or alternative models, as had been previously suggested,[29] did not improve the data. This observation is consistent with our previous study on MXene optical properties[21,28] and other literature reports.[30−32]

The fitting correlation between resistivity and scattering time was checked to determine the best fitting (Figure S2) and to ensure that these parameters can be independently fitted. The resulting optical properties based on these fits are shown in Figure S3. More discussion about the choice of fitting variables and $Ti_3C_2T_x$ MXene optical properties can be found in our previous work.[21,28] The SE fitted results based on these figures are tabulated in Table S1. The fitted results averaged over multiple positions for each film are tabulated in Table S2 and plotted in Figure 1C (filled symbols). These data are in agreement with previous reports.[28,31,33,34]

To further examine the effect of film uniformity and substrate choice,[35] SE mapping measurements were performed on monoflake and multiflake $Ti_3C_2T_x$ MXene films spin-coated on Si substrates (Figures S3 and S4). The averaged values over the entire area of the film (4 cm^2 area) are shown with open symbols in Figure 1C, where the error bars indicate the standard deviation. The larger standard deviation in resistivity of the monoflake films likely arises from the greater heterogeneity in these films. For simplicity, thin films with an average thickness of ∼2 nm are designated as monoflake films in this study. Based on the atomic force microscopy (AFM) results in Figure S5, approximately 61% of the covered surface area of these films was occupied with single flake MXenes with no overlap with other MXenes. More AFM images of the similarly made monoflake MXene films can be found in our previous work.[27] Similarly, films with an average thickness of >20 nm are referred to as multiflake films in the following sections. Nearly all MXene flakes in these films are randomly stacked and overlapped with neighboring flakes.[26,27]

DFT calculations were also performed to gain insight into the mechanisms of charge transport. Previous works have demonstrated that the =O termination is the most thermodynamically stable,[21,27,36] is the predominant termination in experimentally synthesized $Ti_3C_2T_x$ MXenes, and strongly contributes to near-IR optical absorption.[37,38] Therefore, $Ti_3C_2O_2$ MXene was chosen for the calculations presented in this work. In these calculations, the monoflake was modeled as a single flake with periodic boundary conditions only in the in-plane (*xx* and *yy*) direction. To model the multiflake bulk system, multiple single monoflakes were stacked along the *z* direction, with periodic boundary conditions in all directions with a layer of zigzag water inserted between the flakes (see Figure S7 and SI Note S3 for details of this choice). Optical properties were modeled for both the in-plane (*xx*) and out-of-plane (*zz*) directions for the multiflake bulk system. The electron−phonon coupling effects were also considered in the calculation (Note S4 and Figure S10).[39,40]

Effect of Thickness on Resistivity. Figure 1C shows the thickness-dependent resistivity and electron scattering time of as-prepared $Ti_3C_2T_x$ MXene on both SiO_2/Si and Si substrates. Regardless of the substrate and approach, consistent trends in resistivity and scattering times are observed. Moreover, the measured thickness-dependent trends are well beyond the largest measured standard deviation. The

https://doi.org/10.1021/acs.jpclett.5c01439
J. Phys. Chem. Lett. 2025, 16, 7515−7521

corresponding carrier density, diffusion length, and charge mobility data are shown in Figure S8 (more details are in Supplementary Note S1 and Table S2). The results are generally consistent with the previous literature reports.[15,28,41] The slight apparent resistivity increase as a function of the thickness (Figure 1C) arises from the facts that the extinction is not 100% for the thin films and that the measured extinction coefficient, determining the resistivity, represents the value for an effective medium that is only partially filled with the $Ti_3C_2T_x$ MXene as detailed in our previous publication and other reports.[28,42] A similar thickness-dependent resistivity trend was also observed for graphene nanosheets.[43]

The data in Figure 1C show that the electron scattering time decreases with film thickness. Similarly, the carrier mobility and electron diffusion length decrease with increasing film thickness, despite the fact that the carrier density is not affected by the stacking of MXene layers (Figure S8).

A similar increase in resistivity and a decrease in scattering time are observed when comparing the monoflake and the in-plane (xx) component of bulk conductivity in DFT calculations (Figure 1D). The corresponding anisotropic results for both the in-plane (xx) and out-of-plane (zz) components of resistivity and scattering time as well as comparisons for the case without water are shown in Figure S10. It is important to note that the zz resistivity is 3 orders of magnitude higher than that of xx, indicating that the conductivity is predominantly through in-plane charge transport and as such is not included in the data shown in Figure 1D.

Effect of Temperature on Resistivity. To further elucidate the charge transport mechanisms in monoflake and multiflake MXene films, inspired by previous work,[14,16,18] the temperature-dependent resistivity of $Ti_3C_2T_x$ MXene films was measured from room temperature to 873 K in vacuum via SE. As shown in our previous work, under these conditions, MXene films are stable and are not expected to degrade.[27] Unlike annealing in air, which shows a sudden increase in resistivity at 300 °C, indicative of oxidation as evidenced by a temperature-dependent ellipsometry measurement,[27] no such sudden resistivity increase is observed during vacuum annealing at any specific temperature (Figures 2A and 3A), suggesting that oxidation does not occur under vacuum annealing. Detailed structural XRD and XPS characterization after vacuum annealing at 600 °C for 2 h also demonstrated the absence of oxidation products, such as TiO_2.[27] As shown in Figure 2A, completely opposite temperature-dependence trends are seen in the resistivity (R) of the as-prepared monoflake and multiflake $Ti_3C_2T_x$ films (the related carrier mobility results are shown in Figure S11). In agreement with the previous results,[16] the monoflake $Ti_3C_2T_x$ film displays a positive dR/dT, which is consistent with the corresponding theoretical calculations, performed by taking the electron−phonon coupling effects into account (Figure 2B). In contrast, the multiflake $Ti_3C_2T_x$ film displays a negative dR/dT dependence in the experiments (Figure 2A), while the corresponding bulk calculations show a positive trend in both the in-plane (Figure 2B) and out-of-plane (Figure S10C) directions.

The positive dR/dT in experimental monoflakes and in calculated data of both monoflakes and the bulk can be understood as predominantly arising from intraflake charge transport (as schematically shown in the inset of Figure 2A and Figure S12). Given the metallic-like behavior of $Ti_3C_2T_x$, the

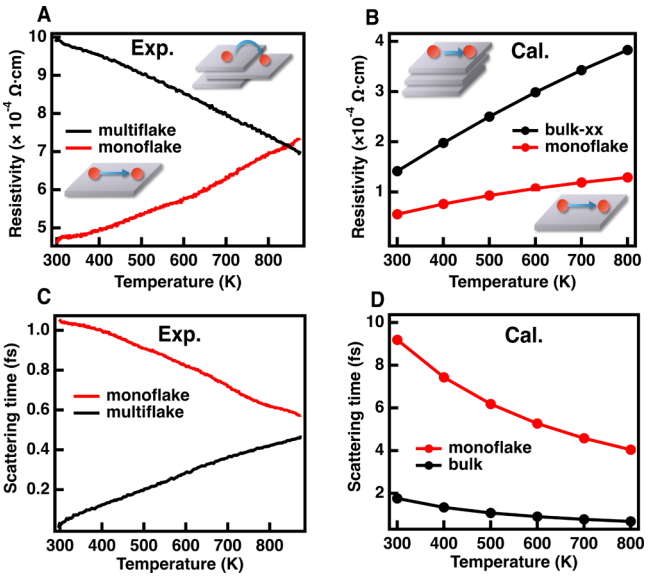

Figure 2. Differences in the charge transport mechanism between monoflakes and multiflakes. (A) Measured temperature-dependent resistivity of as-prepared multiflake (18 nm thick, black) and monoflake (2 nm thick, red) $Ti_3C_2T_x$ films on Si substrates. Insets schematically show the different in-plane charge transport mechanisms in a monoflake (bottom left, intraflake band-like) and multiflake (top right, thermally activated interflake hopping). (B) Calculated temperature-dependent resistivity of a monoflake (red) and in-plane (xx component, black) bulk $Ti_3C_2O_2$ with intercalated water. Insets schematically show the band-like charge transport in the calculated geometry of both monoflakes and in-plane bulk. (C) Measured temperature-dependent electron scattering time of an as-prepared multiflake (black) and monoflake (red) $Ti_3C_2T_x$ films. (D) Calculated temperature-dependent electron scattering time of a monoflake and bulk (with intercalated water) $Ti_3C_2O_2$.

resistivity is expected to increase with temperature, as predicted by the Drude conductivity model. Inside a metal, the intraflake resistivity (denoted by R_{intra}, eq 1) is given as[16,44]

$$R_{intra} \propto \frac{mT}{e^2 n\tau} \tag{1}$$

where m, e, n, and T are the effective electron mass, electron charge, charge carrier density, and temperature, respectively. The electron scattering time (τ) decreases with increasing temperature due to the electron−phonon coupling (Figure 2C,D).[16,45] The decreased carrier mobility of monoflakes with temperature in SE experiments (Figure S8) is also consistent with this picture of the intraflake charge transport mechanism, as the MXene flakes are mostly geometrically separated in monoflake films.

Also consistent with this picture, when the resistivity is calculated without the electron−phonon coupling effect, a negative dR/dT trend is indeed observed (Figure S10A). Here, a relaxation time approximation was adopted, and the scattering time was manually set to τ = 10 fs at all temperatures (as opposed to the temperature-dependent scattering time when including the electron−phonon coupling effect) based on the value obtained in the calculations with the electron−phonon coupling effect (Figure S10D) as well as the previously reported values.[15,41] We note that in calculations without the electron−phonon coupling effect, the electrical conductivity is proportional to the relaxation time. Therefore, using other

https://doi.org/10.1021/acs.jpclett.5c01439
J. Phys. Chem. Lett. 2025, 16, 7515−7521

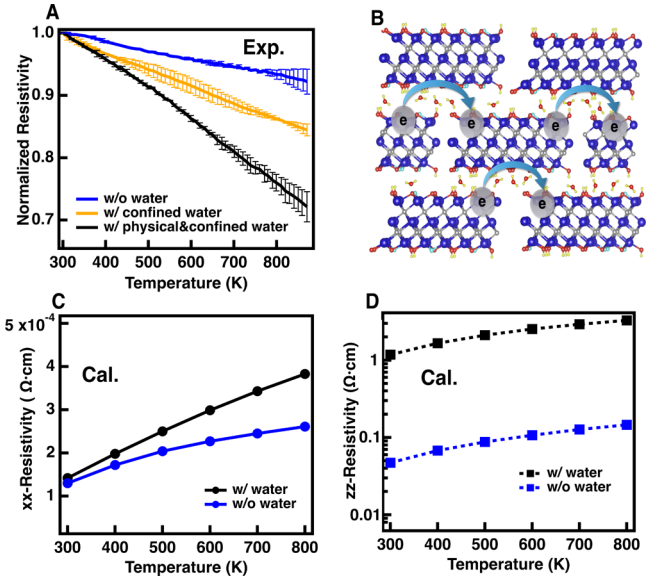

Figure 3. Effects of intercalated water on charge transport. (A) Normalized resistivity of multiflake $Ti_3C_2T_x$ films on the Si substrate vs temperature. Data is shown for an as-prepared multiflake film with both physisorbed and confined water (black curve), a partially annealed film with confined water (orange curve), and a fully annealed film without either confined or physisorbed water (blue curve). The error bars were estimated based on at least two data sets, with each set normalized to its corresponding resistivity at room temperature before averaging. (B) Schematic description of the role of water and surface terminations in assisting the interflake charge transport. (C, D) Calculated in-plane (*xx*) and out-of-plane (*zz*) components of the electrical resistivity of bulk $Ti_3C_2O_2$ without (blue color) and with (black curve) intercalated water vs temperature. The origins of the trend differences in A, C, and D are detailed in the text.

values for the relaxation time does not affect the calculated temperature dependence.

The charge transport mechanism is more complex in multiflake $Ti_3C_2T_x$ films where a negative dR/dT is observed (Figure 2A). In these films, multiple single flakes are randomly stacked along the *z* direction with random lateral displacements, with a wide range of lateral flake sizes, which can also generate numerous boundaries in the *xy* plane. These boundaries are not accounted for in the periodic geometry of the calculated bulk MXene. Under these conditions, thermally activated hopping is expected to contribute to conductivity.[16,44] Given that the out-of-plane resistivity is 3 orders of magnitude higher than the in-plane resistivity (Figures S9 and S10), it is likely that the majority of charge hopping between MXene flakes occurs in the in-plane direction, as schematically shown in the inset of Figure 2A and Figure S12. The temperature dependence of the interflake resistivity (denoted by R_{inter}) can be described by eq 2[16,44]

$$R_{inter} \propto R_0 \exp\left(\frac{T_0}{T}\right)^p \tag{2}$$

where R_0 is a prefactor, T_0 is a characteristic temperature of the thermally activated process related to the activation energy of charge hopping, and p is an exponent that depends on the specific charge hopping mechanism. The carrier mobility is expected to increase with the temperature in a thermally activated hopping mechanism, resulting in increased conductivity and decreased resistivity. It is important to note that the temperature dependence of the intraflake conductivity can add an unknown temperature dependence to R_0 itself, as evidenced by the nonlinear relationship between resistivity and the reciprocal of temperature (Figure S13). However, the effect is mitigated by this strong temperature dependence, resulting in a negative overall trend in dR/dT in the experiments (Figure 2A). As seen in Figure S11, the carrier mobility indeed increases with temperature in multiflake $Ti_3C_2T_x$ films, explaining the positive temperature dependence seen in Figure 2A.

As seen in Figure 2C, the scattering time in multiflake films also increases with temperature, suggesting additional likely contributions from defect trapping in these systems. The Ti and O vacancy defects have been widely reported in $Ti_3C_2T_x$ MXene.[46,47] Defect trapping in multiflake films is also consistent with the thickness-dependent SE results, where shorter electron scattering times, higher resistivity (Figure 1C), and shorter diffusion lengths (Figure S8) are observed as the film thickness is increased. Schematic descriptions of the charge transport in multiflake $Ti_3C_2T_x$ films are illustrated in Figure S9. These results suggest that these defects may be related to edge states as their number increases with the film thickness.

Effect of Water on Resistivity. It has been previously demonstrated that intercalants and surface terminations influence MXene electronic properties.[16] Our previous work demonstrated that trapped water between randomly stacked $Ti_3C_2T_x$ MXene flakes can have a high barrier for removal.[27] While vacuum annealing above 200 °C can remove bulk-like interflake water, the complete removal of confined water and −OH terminations requires vacuum annealing at 600 °C for at least 2 h. We have also previously demonstrated that the MXene morphology does not change after both 200 and 600 °C vacuum annealing, through AFM imaging.[27]

To explore the effects of the trapped and confined water on interflake charge hopping, temperature-dependent SE measurements were performed on $Ti_3C_2T_x$ MXene multiflake films after various vacuum annealing protocols (more details in the Materials and Methods). As shown in Figure 3A, dR/dT decreases when the physisorbed (trapped) water is removed. The complete removal of both confined and physisorbed water further decreases the slope. This trend can be understood by the contribution of water to the interflake resistivity. The mobility of intercalated water molecules increases with temperature, which assists the interflake in-plane charge hopping process as schematically shown in Figure 3B. The additional effects seen upon the removal of confined water also indicate the additional role played by the −OH and −F surface terminations, which are subsequently removed upon high-temperature (>600 °C) vacuum annealing.[48,49] The increased resistivity at high temperature (Figure 3) after −OH removal also aligns with the previous results.[22] Our previous work demonstrates that $Ti_3C_2T_x$ MXenes with −OH and −F terminations exhibit metallic behavior, while those with the =O termination behave more like semiconductors.[21] As such, the OH- and F-terminated MXenes demonstrate higher conductivity than their O-terminated counterparts, consistent with previous DFT calculations.[22] In other words, both the confined water and surface terminations can assist the interflake charge transport, in line with previous reports highlighting the role of water-related hydrogen bonding in charge transport.[50,51]

https://doi.org/10.1021/acs.jpclett.5c01439
J. Phys. Chem. Lett. 2025, 16, 7515−7521

The dR/dT trends are opposite to the experimental data in the calculated bulk $Ti_3C_2O_2$ (Figure 3C,D; more results can be found in Figure S10). This is because, as mentioned previously, in the perfectly periodic geometry of these DFT simulations, lateral boundary hopping is absent, resulting in a dR/dT dependence in bulk simulated films similar to that of monoflakes (Figure 2B,D). As such, the addition of interflake water decreases the in-plane (xx) conductivity and increases the in-plane (xx) resistivity as the temperature is increased (Figure 3C), as water has a negligible effect on the intraflake charge transport of MXene. In contrast, the amplitude of the out-of-plane (zz) resistivity (i.e., 1.2 Ω·cm w/water; 4.7×10^{-2} Ω·cm w/o water at room temperature), while being overall 3 to 4 orders of magnitude higher than the in-plane (xx) resistivity (i.e., 1.4×10^{-4} Ω·cm w/water; 1.3×10^{-4} Ω·cm w/o water at room temperature), decreases dramatically after the removal of water (Figure 3D). Regardless, dR/dT remains positive in both directions with or without water (Figure S10), highlighting the predominant role of intraflake conductivity in the simulated bulk MXenes. In this perfect geometry and with the choice of the intercalated water configuration used in the calculation (Figure S7A and Supplementary Note S3), water, a dielectric material, works as a barrier for charge transport. Upon removal of the water molecules, charge transport is enhanced due to reduced interflake distances and improved induced charge polarization, resulting in decreasing resistivity. This is also consistent with the observation that the out-of-plane resistivity is increased by an order of magnitude when eight water molecules are used in the calculation compared to when only one water molecule is used (Figure S9).

These results further demonstrate that the boundaries or edge states play an important role in understanding the temperature-dependent resistivity trends in MXenes, including the role played by trapped water. It has been theoretically predicated that both armchair and zigzag edges exist for MXenes,[52] which is expected to affect the charge transport as well. More details about the edge states are discussed in our future work.

In addition, the 200 °C vacuum-annealed $Ti_3C_2T_x$ films were shown to retain approximately 90% of their original conductivity after being stored in air for 5 years,[53] demonstrating excellent environmental stability of vacuum-annealed samples. After vacuum annealing at 600 °C to further remove the confined water, the environmental stability of the film is expected to be improved, which will be explored in our future work. Such high environmental stability is highly beneficial for electronic and optoelectronic applications.

In conclusion, spectroscopic ellipsometry measurements and DFT calculations have combined to illuminate the previous debates about the charge transport mechanisms in mono- and multiflake $Ti_3C_2T_x$ MXenes. We reveal that the band-like intraflake transport is dominant in the monoflake and the out-of-plane direction of multiflakes, but the thermally activated hopping controls interflake transport in the in-plane direction of the multiflake, which can be favored by the interflake trapped water. Our results shed light on charge transport mechanisms in $Ti_3C_2T_x$ MXenes, opening avenues for further exploration in electronic and optoelectronic applications, especially in extreme high-temperature environments.

■ ASSOCIATED CONTENT

Supporting Information

The Supporting Information is available free of charge at https://pubs.acs.org/doi/10.1021/acs.jpclett.5c01439.

Materials and Methods; Supplementary Notes: SE data modeling and DFT details; Tables S1 and S2; and Figures S1−S13 (PDF)

■ AUTHOR INFORMATION

Corresponding Authors

Babak Anasori − *School of Materials Engineering and School of Mechanical Engineering, Purdue University, West Lafayette, Indiana 47907, United States;* orcid.org/0000-0002-1955-253X; Email: banasori@purdue.edu

Andrew M. Rappe − *Department of Chemistry, University of Pennsylvania, Philadelphia, Pennsylvania 19104, United States;* orcid.org/0000-0003-4620-6496; Email: rappe@sas.upenn.edu

Zahra Fakhraai − *Department of Chemistry, University of Pennsylvania, Philadelphia, Pennsylvania 19104, United States;* orcid.org/0000-0002-0597-9882; Email: fakhraai@sas.upenn.edu

Authors

Hui Fang − *Department of Chemistry, University of Pennsylvania, Philadelphia, Pennsylvania 19104, United States;* orcid.org/0000-0002-4024-1234

Zhenyao Fang − *Department of Chemistry, University of Pennsylvania, Philadelphia, Pennsylvania 19104, United States;* orcid.org/0000-0001-6841-3934

Anupma Thakur − *School of Materials Engineering, Purdue University, West Lafayette, Indiana 47907, United States;* orcid.org/0000-0001-7897-9229

Complete contact information is available at: https://pubs.acs.org/10.1021/acs.jpclett.5c01439

Author Contributions

[§]H.F. and Z.F. contributed equally to this work.

Notes

The authors declare no competing financial interest.

■ ACKNOWLEDGMENTS

The authors acknowledge funding support from the U.S. National Science Foundation, award number CMMI-2134607. Z. Fang acknowledges funding from the U.S. National Science Foundation, award number CHE-2303044. H.F. acknowledges the School of Arts and Sciences at the University of Pennsylvania for the Postdoctoral Fellowship. Z. Fang thanks Dr. Zhenbang Dai for helpful discussions on electron−phonon coupling calculations. Z. Fakhraai and H.F. thank Prof. Alexandra Vojvodic for her helpful insight and discussions. The authors acknowledge Lianne Beltran for professional editing.

■ REFERENCES

(1) VahidMohammadi, A.; Rosen, J.; Gogotsi, Y. The world of two-dimensional carbides and nitrides (MXenes). *Science* **2021**, *372*, No. eabf1581.

(2) Hantanasirisakul, K.; Zhao, M.-Q.; Urbankowski, P.; Halim, J.; Anasori, B.; Kota, S.; Ren, C. E.; Barsoum, M. W.; Gogotsi, Y. Fabrication of $Ti_3C_2T_x$ MXene transparent thin films with tunable

optoelectronic properties. *Advanced Electronic Materials* **2016**, *2*, 1600050.
(3) Lyu, B.; Kim, M.; Jing, H.; Kang, J.; Qian, C.; Lee, S.; Cho, J. H. Large-area MXene electrode array for flexible electronics. *ACS Nano* **2019**, *13*, 11392−11400.
(4) Naguib, M.; Kurtoglu, M.; Presser, V.; Lu, J.; Niu, J.; Heon, M.; Hultman, L.; Gogotsi, Y.; Barsoum, M. W. Two-dimensional nanocrystals produced by exfoliation of Ti_3AlC_2. *Adv. Mater.* **2011**, *23*, 4248−4253.
(5) Hantanasirisakul, K.; Gogotsi, Y. Electronic and optical properties of 2D transition metal carbides and nitrides (MXenes). *Adv. Mater.* **2018**, *30*, 1804779.
(6) Gogotsi, Y.; Anasori, B. The rise of MXenes. *ACS Nano* **2019**, *13*, 8491−8494.
(7) Naguib, M.; Barsoum, M. W.; Gogotsi, Y. Ten years of progress in the synthesis and development of MXenes. *Adv. Mater.* **2021**, *33*, 2103393.
(8) Gogotsi, Y. The Future of MXenes. *Chem. Mater.* **2023**, *35*, 8767−8770.
(9) Li, X.; Huang, Z.; Shuck, C. E.; Liang, G.; Gogotsi, Y.; Zhi, C. MXene chemistry, electrochemistry and energy storage applications. *Nature Reviews Chemistry* **2022**, *6*, 389−404.
(10) Anasori, B.; Lukatskaya, M. R.; Gogotsi, Y. 2D metal carbides and nitrides (MXenes) for energy storage. *Nature Reviews Materials* **2017**, *2*, 16098−1.
(11) Johnson, L. R.; Sridhar, S.; Zhang, L.; Fredrickson, K. D.; Raman, A. S.; Jang, J.; Leach, C.; Padmanabhan, A.; Price, C. C.; Frey, N. C. MXene materials for the electrochemical nitrogen reduction—functionalized or not? *ACS Catal.* **2020**, *10*, 253−264.
(12) Miranda, A.; Halim, J.; Barsoum, M.; Lorke, A. Electronic properties of freestanding $Ti_3C_2T_x$ MXene monolayers. *Appl. Phys. Lett.* **2016**, *108*, 033102.
(13) Xu, X.; Guo, T.; Lanza, M.; Alshareef, H. N. Status and prospects of MXene-based nanoelectronic devices. *Matter* **2023**, *6*, 800−837.
(14) Zheng, W.; Sun, B.; Li, D.; Gali, S. M.; Zhang, H.; Fu, S.; Di Virgilio, L.; Li, Z.; Yang, S.; Zhou, S. Band transport by large Fröhlich polarons in MXenes. *Nat. Phys.* **2022**, *18*, 544−550.
(15) Zhao, T.; Xie, P.; Wan, H.; Ding, T.; Liu, M.; Xie, J.; Li, E.; Chen, X.; Wang, T.; Zhang, Q. Ultrathin MXene assemblies approach the intrinsic absorption limit in the 0.5−10 THz band. *Nat. Photonics* **2023**, *17*, 622−628.
(16) Hart, J. L.; Hantanasirisakul, K.; Lang, A. C.; Anasori, B.; Pinto, D.; Pivak, Y.; van Omme, J. T.; May, S. J.; Gogotsi, Y.; Taheri, M. L. Control of MXenes' electronic properties through termination and intercalation. *Nat. Commun.* **2019**, *10*, 522.
(17) Jing, Z.; Liu, J.; Li, N.; Wang, H.; Wu, K.; Cheng, Y.; Xiao, B. Electron-phonon scattering limited intrinsic electrical conductivity of metallic MXenes X_2C(X= Ti or Mo). *J. Phys. D: Appl. Phys.* **2021**, *54*, 015301.
(18) Han, M.; Maleski, K.; Shuck, C. E.; Yang, Y.; Glazar, J. T.; Foucher, A. C.; Hantanasirisakul, K.; Sarycheva, A.; Frey, N. C.; May, S. J. Tailoring electronic and optical properties of MXenes through forming solid solutions. *J. Am. Chem. Soc.* **2020**, *142*, 19110−19118.
(19) Lipatov, A.; Bagheri, S.; Sinitskii, A. Metallic Conductivity of $Ti_3C_2T_x$ MXene Confirmed by Temperature-Dependent Electrical Measurements. *ACS Materials Letters* **2024**, *6*, 298−307.
(20) Wang, P.; Tang, J.; Yang, Y.; Guo, J.; Hu, B.; Cui, S.; Wang, X.; Xu, B. Thickness-dependent optoelectronic properties of titanium carbide MXene. *Mater. Lett.* **2024**, *358*, 135862.
(21) Fang, H.; Fang, Z.; Thakur, A.; Rad, V.; Chandran, N.; Michałowski, P.; Soroush, M.; Anasori, B.; Rappe, M. A.; Fakhraai, Z. Why $Ti_3C_2T_x$ MXenes Are Conductive but Not Plasmonic in the Optical Domain. *ChemRxiv* 2024, 12−13 DOI: 10.26434/chemrxiv-2024-rpf17-v2.
(22) Khanal, R.; Irle, S. Effect of surface functional groups on MXene conductivity. *J. Chem. Phys.* **2023**, *158*, 194701.
(23) Lounasvuori, M.; Zhang, T.; Gogotsi, Y.; Petit, T. Tuning the Microenvironment of Water Confined in $Ti_3C_2T_x$ MXene by Cation Intercalation. *J. Phys. Chem. C* **2024**, *128*, 2803−2813.
(24) Arole, K.; Pas, S. E.; Thakur, R. M.; Amiouny, L. A.; Kabir, M. H.; Dujovic, M.; Radovic, M.; Lutkenhaus, J. L.; Green, M. J.; Liang, H. Effects of Intercalation on ML-$Ti_3C_2T_z$ MXene Properties and Friction Performance. *ACS Appl. Mater. Interfaces* **2024**, *16*, 64156−64165.
(25) Mathis, T. S.; Maleski, K.; Goad, A.; Sarycheva, A.; Anayee, M.; Foucher, A. C.; Hantanasirisakul, K.; Shuck, C. E.; Stach, E. A.; Gogotsi, Y. Modified MAX phase synthesis for environmentally stable and highly conductive Ti_3C_2 MXene. *ACS Nano* **2021**, *15*, 6420−6429.
(26) Thakur, A.; Chandran, B.S. N.; Davidson, K.; Bedford, A.; Fang, H.; Im, Y.; Kanduri, V.; Wyatt, B. C.; Nemani, S. K.; Poliukhova, V.; Kumar, R.; Fakhraai, Z.; Anasori, B. Step-by-Step Guide for Synthesis and Delamination of $Ti_3C_2T_x$ MXene. *Small Methods* **2023**, *7*, 2300030.
(27) Fang, H.; Thakur, A.; Zahmatkeshsaredorahi, A.; Fang, Z.; Rad, V.; Shamsabadi, A.; Ahmad; Pereyra, C.; Soroush, M.; Rappe, M. A.; Xu, G. X.; Anasori, B.; Fakhraai, Z. Stabilizing $Ti_3C_2T_x$ MXene Flakes in Air by Removing Confined Water. *Proc. Natl. Acad. Sci. U. S. A.* **2024**, *121*, No. e2400084121.
(28) Shamsabadi, A. A.; Fang, H.; Zhang, D.; Thakur, A.; Chen, C. Y.; Zhang, A.; Wang, H.; Anasori, B.; Soroush, M.; Gogotsi, Y.; Fakhraai, Z. The Evolution of MXenes Conductivity and Optical Properties Upon Heating in Air. *Small Methods* **2023**, *7*, 2300568.
(29) Furchner, A.; Parker, T.; Mauchamp, V.; Hurand, S.; Plaickner, J.; Rappich, J.; Emerenciano, A. A.; Hinrichs, K.; Gogotsi, Y.; Petit, T. $Ti_3C_2T_x$ MXene Thin Films and Intercalated Species Characterized by IR-to-UV Broadband Ellipsometry. *J. Phys. Chem. C* **2025**, *129*, 500−507.
(30) Panova, D. A.; Tselikov, G. I.; Ermolaev, G. A.; Syuy, A. V.; Zimbovskii, D. S.; Kapitanova, O. O.; Yakubovsky, D. I.; Mazitov, A. B.; Kruglov, I. A.; Vyshnevyy, A. A. Broadband optical properties of Ti_3C_2 MXene revisited. *Opt. Lett.* **2024**, *49*, 25−28.
(31) Dillon, A. D.; Ghidiu, M. J.; Krick, A. L.; Griggs, J.; May, S. J.; Gogotsi, Y.; Barsoum, M. W.; Fafarman, A. T. Highly conductive optical quality solution-processed films of 2D titanium carbide. *Adv. Funct. Mater.* **2016**, *26*, 4162−4168.
(32) Murray, S. L.; Serajian, S.; Gnani Peer Mohamed, S. I.; Robinson, S.; Krishnamoorthy, R.; Das, S. R.; Bavarian, M.; Nejati, S.; Kilic, U.; Schubert, M. Ultrabroadband Optical Properties of 2D Titanium Carbide MXene. *ACS Appl. Mater. Interfaces* **2024**, *16*, 70763−70773.
(33) Chaudhuri, K.; Alhabeb, M.; Wang, Z.; Shalaev, V. M.; Gogotsi, Y.; Boltasseva, A. Highly broadband absorber using plasmonic titanium carbide (MXene). *ACS Photonics* **2018**, *5*, 1115−1122.
(34) Lioi, D. B.; Stevenson, P. R.; Seymour, B. T.; Neher, G.; Schaller, R. D.; Gosztola, D. J.; Vaia, R. A.; Vernon, J. P.; Kennedy, W. J. Simultaneous Ultrafast Transmission and Reflection of Nanometer-Thick $Ti_3C_2T_x$ MXene Films in the Visible and Near-Infrared: Implications for Energy Storage, Electromagnetic Shielding, and Laser Systems. *ACS Applied Nano Materials* **2020**, *3*, 9604−9609.
(35) Agulto, V. C.; Iwamoto, T.; Zhao, Z.; Liu, S.; Kato, K.; Nakajima, M. Wafer-scale mapping of carrier density and mobility with terahertz time-domain ellipsometry. *Opt. Lett.* **2025**, *50*, 948−951.
(36) Fredrickson, K. D.; Anasori, B.; Seh, Z. W.; Gogotsi, Y.; Vojvodic, A. Effects of applied potential and water intercalation on the surface chemistry of Ti_2C and Mo_2C MXenes. *J. Phys. Chem. C* **2016**, *120*, 28432−28440.
(37) Hu, T.; Li, Z.; Hu, M.; Wang, J.; Hu, Q.; Li, Q.; Wang, X. Chemical origin of termination-functionalized MXenes: $Ti_3C_2T_2$ as a case study. *J. Phys. Chem. C* **2017**, *121*, 19254−19261.
(38) Liu, N.; Li, Q.; Wan, H.; Chang, L.; Wang, H.; Fang, J.; Ding, T.; Wen, Q.; Zhou, L.; Xiao, X. High-temperature stability in air of $Ti_3C_2T_x$ MXene-based composite with extracted bentonite. *Nat. Commun.* **2022**, *13*, 5551.

https://doi.org/10.1021/acs.jpclett.5c01439
J. Phys. Chem. Lett. 2025, 16, 7515−7521

(39) Wang, A.; Li, S.; Zhang, X.; Bao, H. Roles of electrons on the thermal transport of 2D metallic MXenes. *Physical Review Materials* **2022**, *6*, 014009.
(40) Zhang, Q.; Li, J.; Wen, J.; Li, W.; Chen, X.; Zhang, Y.; Sun, J.; Yan, X.; Hu, M.; Wu, G. Simultaneous capturing phonon and electron dynamics in MXenes. *Nat. Commun.* **2022**, *13*, 7900.
(41) Li, G.; Kushnir, K.; Dong, Y.; Chertopalov, S.; Rao, A. M.; Mochalin, V. N.; Podila, R.; Titova, L. V. Equilibrium and non-equilibrium free carrier dynamics in 2D $Ti_3C_2T_x$ MXenes: THz spectroscopy study. *2D Materials* **2018**, *5*, 035043.
(42) Walther, M.; Cooke, D.; Sherstan, C.; Hajar, M.; Freeman, M.; Hegmann, F. Terahertz conductivity of thin gold films at the metal-insulator percolation transition. *Phys. Rev. B* **2007**, *76*, 125408.
(43) Fang, X.-Y.; Yu, X.-X.; Zheng, H.-M.; Jin, H.-B.; Wang, L.; Cao, M.-S. Temperature-and thickness-dependent electrical conductivity of few-layer graphene and graphene nanosheets. *Phys. Lett. A* **2015**, *379*, 2245−2251.
(44) Halim, J.; Moon, E. J.; Eklund, P.; Rosen, J.; Barsoum, M. W.; Ouisse, T. Variable range hopping and thermally activated transport in molybdenum-based MXenes. *Phys. Rev. B* **2018**, *98*, 104202.
(45) Kasap, S. O. *Electronic Materials and Devices*; McGraw-Hill: New York, 2006.
(46) Sang, X.; Xie, Y.; Lin, M.-W.; Alhabeb, M.; Van Aken, K. L.; Gogotsi, Y.; Kent, P. R.; Xiao, K.; Unocic, R. R. Atomic defects in monolayer titanium carbide ($Ti_3C_2T_x$) MXene. *ACS Nano* **2016**, *10*, 9193−9200.
(47) Zhang, Y.; Zhao, Q.; Danil, B.; Xiao, W.; Yang, X. Oxygen-Vacancy-Induced Formation of Pt-Based Intermetallics on MXene with Strong Metal-Support Interactions for Efficient Oxygen Reduction Reaction. *Adv. Mater.* **2024**, *36*, 2400198.
(48) Persson, I.; Näslund, L.-Å.; Halim, J.; Barsoum, M. W.; Darakchieva, V.; Palisaitis, J.; Rosen, J.; Persson, P. O. Å. On the organization and thermal behavior of functional groups on Ti_3C_2 MXene surfaces in vacuum. *2D Materials* **2018**, *5*, 015002.
(49) El-Demellawi, J. K.; Lopatin, S.; Yin, J.; Mohammed, O. F.; Alshareef, H. N. Tunable multipolar surface plasmons in 2D $Ti_3C_2T_x$ MXene flakes. *ACS Nano* **2018**, *12*, 8485−8493.
(50) Yang, W.-Y.; Zheng, J.; Zhang, X.-G.; Chen, L.-C.; Si, Y.; Huang, F.-Z.; Hong, W. Charge transport through a water-assisted hydrogen bond in single-molecule glutathione disulfide junctions. *Journal of Materials Chemistry C* **2020**, *8*, 481−486.
(51) Duo, H.; Wang, H.; Shima, S.; Takamura, E.; Sakamoto, H. Hydrogen-bond enhanced interior charge transport and trapping in all-fiber triboelectric nanogenerators for human motion sensing and communication. *Nano Energy* **2024**, *131*, 110297.
(52) Hong, L.; Klie, R. F.; Öğüt, S. First-principles study of size-and edge-dependent properties of MXene nanoribbons. *Phys. Rev. B* **2016**, *93*, 115412.
(53) Lee, A.; Shekhirev, M.; Anayee, M.; Gogotsi, Y. Multi-year study of environmental stability of $Ti_3C_2T_x$ MXene films. *Graphene and 2D materials* **2024**, *9*, 77−85.

https://doi.org/10.1021/acs.jpclett.5c01439
J. Phys. Chem. Lett. 2025, 16, 7515−7521